EFDA–JET–PR(10)02

M. Gatu Johnson, S. Conroy, M. Cecconello, E. Andersson Sundén, G. Ericsson, M. Gherendi, C. Hellesen, A. Hjalmarsson, A. Murari, S. Popovichev, E. Ronchi, M. Weiszflog, V. L Zoita and JET EFDA contributors

Modelling and TOFOR Measurements of Scattered Neutrons at JET

Modelling and TOFOR Measurements of Scattered Neutrons at JET

M. Gatu Johnson[1], S. Conroy[1], M. Cecconello[1], E. Andersson Sundén[1], G. Ericsson[1], M. Gherendi[2], C. Hellesen[1], A. Hjalmarsson[1], A. Murari[3], S. Popovichev[4], E. Ronchi[1], M. Weiszflog[1], V.L. Zoita[2] and JET EFDA contributors*

JET-EFDA, Culham Science Centre, OX14 3DB, Abingdon, UK

[1] EURATOM-VR Association, Department of Physics and Astronomy, Uppsala University, Box 516, SE-75120 Uppsala, Sweden
[2] Association EURATOM-MEdC, National Institute for Laser, Plasma and Radiation Physics, Bucharest, Romania
[3]Consorzio RFX-Associazione EURATOM ENEA per la Fusione, I-35127 Padova, Italy
[4]EURATOM-CCFE Fusion Association, Culham Science Centre, OX14 3DB, Abingdon, OXON, UK
** See annex of F. Romanelli et al, "Overview of JET Results", (Proc. 22 [nd] IAEA Fusion Energy Conference, Geneva, Switzerland (2008)).*

Preprint of Paper to be submitted for publication in
Plasma Physics and Controlled Fusion

ABSTRACT

In this paper, the scattered and direct neutron fluxes in the line-of-sight of the TOFOR neutron spectrometer at JET are simulated and the simulations compared with measurement results. The Monte Carlo code MCNPX is used in the simulations, with a vessel material composition obtained from the JET drawing office and neutron emission profiles calculated from TRANSP simulations of beam ion density profiles. The MCNPX simulations show that the material composition of the scattering wall has a large effect on the shape of the scattered neutron spectrum. Neutron source profile shapes as well as radial and vertical source displacements in the TOFOR line-of-sight are shown to only marginally affect the scatter, while having a larger impact on the direct neutron flux. A matrix of simulated scatter spectra for mono-energetic source neutrons is created which is folded with an approximation of the source spectrum for each JET pulse studied to obtain a scatter component for use in the data analysis. The scatter components thus obtained are shown to describe the measured data. It is also demonstrated that the scattered flux is approximately constant relative to the total neutron yield as measured with the JET fission chambers, while there is a larger spread in the direct flux, consistent with simulations. The simulated effect on the integrated scattered/direct ratio of an increase with movements outward along the radial direction and a drop at higher values of the vertical plasma position is also reproduced in the measurements. Finally, the quantitative agreement found in scatter/direct ratios between simulations (0.185±0.005) and measurements (0.187±0.050) serves as a solid benchmark of the MCNPX model used.

1. INTRODUCTION

The issue of energy degraded neutrons that have scattered off the fusion tokamak vessel wall before reaching the detecting instrument, here referred to as scattered neutrons but also sometimes as wall emission neutrons, is important because it has an impact on the analysis of collected neutron data. The scattered neutrons can be contrasted with direct neutrons, which are detected without undergoing scattering with a corresponding loss of energy on the way from the plasma source. Obviously, in a tokamak operating with DT fuel, measurements of 2.5MeV neutrons from $d+d \rightarrow {}^{3}He+n$ reactions will be affected by the flux of scattered 14MeV neutrons from $d+t \rightarrow {}^{4}He+n$ reactions. Maybe less obvious but no less important is the fact that a fraction of the energy-degraded scattered neutrons fall very close in energy to the direct emission peak; this affects the possibility to accurately determine the neutron rate and, consequently, the fusion power produced.

The impact of scattered neutrons on tokamak neutron measurements has been recognized in previous work at JET [3] and TFTR [4] and in preparations for ITER [5, 6, 7 ,8, 9]. In [1], the possibility of separation of scattered neutrons from direct ones is claimed to be vital for the successful operation of the JET neutron profile monitor. Ref [2] discusses observations of scattered neutrons on TFTR, where the scattered flux is determined to be 30 percent if so-called see through collimators are not used. Scattered and direct neutron simulations for the plasma focus device PF-1000 are described in [10], where it is shown that accurate analysis of collected neutron spectra would require

scattered neutrons to be taken into account. In [11], the authors anticipate that the advent of more advanced neutron spectrometers will make the scattered flux a limiting factor in the accuracy of neutron spectral analysis. With the installation of the TOFOR neutron spectrometer [12] at JET, this prediction was realized. A significant contribution to the neutron spectrum as measured with TOFOR was seen that could only be explained in terms of scatter and that had to be accounted for in order to accurately analyze the data. Preliminary TOFOR scatter results were presented in [13]. In ref [9], Antozzi *et al*. report on a thorough study of the expected scattered neutron flux from 14MeV neutrons in a large tokamak using MCNP simulations. Scatter on carbon and iron nuclei is investigated independently and the scattered flux is analyzed in terms of contributions from single scattering, in-board and out-board multiple scattering. The study focuses on a hypothetical example with a horizontal radial line-of-sight. Changes in the scattered flux depending on plasma width, plasma elongation, horizontal and vertical displacements are studied and it is concluded that, given the radial viewing geometry, the largest impact on the magnitude of the scattered flux is from displacement in the radial direction. The authors also discuss the fact that the shape of the scattered neutron spectrum will be highly sensitive to wall nuclide composition and plasma temperature (in the case of a burning thermonuclear plasma). It is concluded that the temperature must be well known in order to perform accurate subtraction of the scattered neutrons, and that the magnitude of the scattered flux could be measured in the region of little or no direct plasma emission, given a large enough "energy bite" of the detecting instrument.

In this paper, we take the practical approach of focusing on what the scattered neutron spectrum as detected with TOFOR should look like according to simulations, how sensitive it is to parameter variations and how it can be accounted for in the analysis of measured data. MCNPX 2.5 [14] is used in the simulations and the results are compared to ref [9] when relevant to verify consistency. We will show how the correction for the scattered neutron flux can be done in the analysis of TOFOR data in the general case of applied auxiliary heating and rather complex neutron spectra without prior knowledge of the 'temperature' (or equivalent spectral shape) by creating a matrix of expected scatter spectra as a function of direct neutron energy, folding this with an approximation of the direct spectrum from the data and iterating until a scatter component of the correct shape is produced. A comparison between scatter/direct neutron ratios in the TOFOR line-of-sight as predicted from MCNPX simulations (0.185±0.005) and determined from analysis of experimental TOFOR data (0.187±0.050) serves as a benchmark to verify the reliability of the MCNPX model.

2. TOFOR

TOFOR is a time-of-flight neutron spectrometer in regular operation at JET since 2005. It is optimized for study of 2.5MeV neutrons from deuterium plasmas but has a large dynamic range allowing for detection of neutrons in a large energy range including, e.g., 14MeV neutrons from deuterium-tritium reactions. The neutron flight time is measured between a primary set of five small in-beam scintillator detectors and a secondary set of 32 larger, removed scintillator detectors. Time-of-flight

(t_{TOF}) spectra are reconstructed post-discharge from time traces of individual events from all 37 detectors. True events corresponding to interaction of the same neutron in both detector sets as well as random events representing a combination of uncorrelated neutrons will be constructed in this way. The randoms will show up as a flat intensity level across the spectrum which can be accurately determined and accounted for through analysis of data in the unphysical region of negative t_{TOF}.

To lowest order, an incident neutron energy E_n (MeV) will manifest itself as a coincidence with a flight time $t_{TOF} = 1.02 \cdot 10^2 \, En^{-1/2}$ ns; for example, 2.5MeV neutrons will have flight times around 65ns. This simple approximation must then be modified to account for the finite size of the detectors and for neutrons undergoing multiple scattering on their way between the two detector sets. Such effects are included in the TOFOR response function [15], simulated using GEANT4 in the range $E_n = 1 - 18$MeV. As an example, the simulated response for quasi-monoenergetic 2.45±0.025MeV neutrons is shown in Figure 1. Both the broadening of the peak due to the instrument geometry and the multiscatter tails on the low and high time of flight sides of the peak are clearly seen.

The detection efficiency of TOFOR is energy dependent, due both to the cross section of the *n,p* reaction invoked for neutron detection in the scintillator material and to the geometric configuration of the setup. It is also dependent on the setting of discriminator thresholds in the data acquisition electronics. We have aimed at setting the thresholds to $E_p = 380$keV to get 100% efficiency for detection of 2.5MeV neutrons on a direct path between the two detector sets while discriminating against low energy noise. However, we estimate an uncertainty in the threshold settings of $\Delta E_p = \pm 60$ keV, leading to the uncertainty in the detector response shown in Figure 1 and a corresponding uncertainty in the energy-dependent efficiency as shown in Figure 2.

The response function of TOFOR is essential in the interpretation of scattered neutron results. Any measurement of energy-degraded scatter will be intermixed with multiscatter events in the region of the spectrum with high t_{TOF} (Figure 1), since lower incident energy means longer flight times. For accurate determination of the scattered neutron flux, the response needs to be well characterized in terms of threshold levels. As can be seen, the current intrinsic uncertainty in the discriminator threshold determination process ($\Delta E_p = \pm 60$keV) leads to a sizable span in multiscatter level (Figure 1). For TOFOR, we have also observed drifts in PM tube gain over time, leading to a further uncertainty in effective threshold levels which needs to be taken into account. TOFOR has been operational and collected data for some 10,000 JET pulses. In this paper, we chose to focus on the pulse interval 71650-74000, with well characterized response.

When comparing simulated and measured scatter, also the energy dependent efficiency (Figure 2) as determined from the response function simulations will play a role. The backscatter will include a spectrum of different neutron energies. Since the efficiency of TOFOR goes to zero at 1 MeV, this constitutes the low energy detection threshold. When comparing measured and simulated spectra, this has been taken into account by setting a lower E_n limit at 1 MeV.

TOFOR views the plasma radially through a vertical Line-Of-Sight (LOS) from its location in the JET roof laboratory (Figure 3a). The sight line is defined by the collimator through the roof

laboratory floor, a concrete precollimator structure that can be adjusted to change the viewing cone of TOFOR, and the upper vertical port on the JET vessel. To create an accurate MCNPX model for determination of the scattered flux reaching TOFOR, detailed knowledge of the sight line is essential. This is not a straight-forward task since the coordinate systems for the JET torus hall and roof laboratory are not linked. We base our estimate on

- drawings giving the vertical distances between different structures in the sight line,
- a theodolite survey done during TOFOR installation that determined the instrument axis and hence viewing angle to be tilted 1^{o} relative to the true vertical and
- a sight line survey also done during installation, that gave (i) the intersection point at the vertical port (as drawn on a piece of mm paper glued to the port) and (ii) the setting of the precollimator that corresponded to blocking half the line-of-sight of TOFOR (outer jaw at 54.5mm).

The vertical distances as given by drawings are shown in Figure 3b. The inner and outer radial jaws of the TOFOR precollimator are fully open when set to 152.5 and 143.3mm, respectively. From these numbers, we calculate that the field-of-view as seen from the TOFOR primary detector centre point extends in the radial direction from 2.74 to 3.02m major radius, centred at 2.88m, at the torus midplane. If the sight line was limited only by the collimator through the roof laboratory floor, the field of view would be 44 cm wide. In practice, the limiting structures according to our calculations are the precollimator on the outboard and the vertical port on the inboard sides, respectively.

The field of view is restricted also in the toroidal direction, by the precollimator (with a 70.6+71.5mm wide opening) and the vertical port. The vertical port is not symmetric in the toroidal direction but wider on the outboard side and narrower on the inboard side. A simple code has been written where the radial footprint of TOFOR at the torus midplane is calculated neglecting the toroidal variations (Figure 4). The code takes into account the assumed block of the sight line by the precollimator and the vertical port as well as the roof laboratory floor collimator.

The uncertainty in especially the half-view precollimator setting estimated in the TOFOR installation survey (54.5mm) is expected to be large. An error in this number would propagate through the calculations to have a large impact on the LOS estimate. A validation of the estimated LOS can be obtained by comparing with measurements using a 2D array of super heated fluid detectors (SHFDs, [16]) placed above TOFOR in the roof laboratory (Figure 3b). The code used to produce Figure 4 can be applied to calculate the expected footprint of a flat neutron emission profile at the estimated SHFD array location 3.5m above TOFOR. The calculation is done for a fully open (143.3mm) precollimator, one set to 82.7 and one set to 22.7mm. The results are shown in Figure 5 (lines). These calculated footprints can be compared with measurements using SHFD for pulses with the same precollimator settings, also shown in Figure 5 (points with error bars). Two important points should be remembered when comparing calculations and measurements: (i) While the neutron emission profiles for the calculations were assumed flat in the LOS, this was in all likelihood not the case for the experimental data. (ii) The estimated distance of 3.5m between

the roof laboratory floor and the location of the SHFDs comes with a large uncertainty. Still, the agreement between measurements and calculations is remarkable, lending credit to our estimate of the TOFOR line-of-sight.

3. SIMULATIONS

The MCNPX model used in the simulation is a full model of the JET torus with the divertor, vertical port, precollimator and roof laboratory collimator included as shown in Figure 6a. In the model, we take into account the sight line information as described in section 2. By necessity the modelling includes simplifications; only parts of the vessel with a direct impact in the TOFOR line of sight are modelled in detail. In Figure 6b, a close-up of the vessel cross section is shown to demonstrate the level of detail included. A point detector at the location of the TOFOR primary detector is used to tally total and uncollided (direct) neutron fluxes as functions of energy. The scattered neutron flux is taken to be the collided neutron flux, obtained through subtraction of the uncollided flux from the total.

Taking the geometry (shown in Figure 6) as given, assumptions that affect the results of the simulations have to be made on

- the material composition for each model component,
- the plasma shape in terms of an assumed neutron emission profile,
- the radial plasma position, and
- the vertical plasma position.

Below, the effect of each of these assumptions on the shape of the scatter component and the relative intensity scatter/direct is discussed. For each of these investigations, a quasi-monoenergetic neutron source with $E_n = 2.5 \pm 0.025$MeV is used.

3.1. EFFECT OF MATERIAL COMPOSITION IN MODEL

In the preliminary work on TOFOR backscatter presented in [11], a simplified MCNPX model of JET excluding the divertor structure was used. The lower vertical port (Figure 3a) was filled with inconel and a 1cm layer of carbon was added to on the bottom of the JET vessel account for the divertor carbon tiles. The thickness of this layer was adjusted to give a component shape that matched TOFOR data from thermonuclear (so called ohmic) JET pulses. For the current model, we have obtained information on the material composition of the various model components from the JET drawing office. Based on this information, we conclude that the main constituents of the JET divertor region most relevant for our application are Ni (the dominant element in the inconel of the support structures) and C (dominant in the divertor tiles). In the model, the divertor tiles contain 95% C and 5% inconel by weight (as do all tiles indicated with purple colour in Figure 6b), support tiles contain inconel only (green) and "composite" tiles contain a mixture of elements, dominated by copper (light blue); these latter tiles include e.g. the divertor coils. The density of the carbon tiles has been adjusted to include a contribution from their inconel supports. Our best efforts have been put into

making the model as accurate a description of the vessel as possible; however, the information obtained from the drawing office has been modified in some aspects to reach a level of detail which is a compromise between accuracy and practicality.

In order to clarify the influence of the two main materials, we have also looked at results from a model containing a larger fraction of Ni relative to C (divertor tiles with 34% C and 66% inconel by weight). In Figure 7, three sets of results are presented: the ones obtained in the preliminary study of ref [11], the high Ni model and the "drawing office" model as outlined above (and in Figure 6). In order to interpret the results, we note that the energy loss to the recoil nucleus in an elastic scattering event will be [17]

$$E_R = \frac{4A}{(1+A)^2} \ (\cos^2 \theta) \ E_n, \qquad (1)$$

where A is the mass number of the nucleus, q the scattering angle and En the incident neutron energy. Scattering at about 180^o angles will dominate due to the viewing geometry. The peaks observable in Figure 7 can thus be identified as resulting from elastic scattering on ^{12}C (at about 1.8MeV) and ^{58}Ni (at about 2.3MeV). The peak at 2.5MeV representing very small energy losses is due to inscatter, while the structure below 1MeV is due to inelastic scattering involving excited states of various inconel constituents.

As can be seen in Figure 7, the impact of the material composition on the spectral shape of the scattered neutrons is large. The uncertainty in the information obtained from the drawing office for implementation in our model and in the implementation itself (due to the selected level of detail) can have an impact on the shape of the spectrum and should be kept in mind when assessing the results. This is in agreement with the conclusion reached by Antozzi et al [9], i.e., that straight-forward computation of the scattered neutron spectrum might never reach the desired accuracy specifically due to indetermination of the nuclide composition of the wall.2 Effect of different plasma shapes

In [11], the neutron emitting JET plasma was approximated as a toroidal neutron source with a square poloidal cross section of 1m sides. Here, we investigate the impact of using a realistic neutron emission profile based on actual JET plasma configurations. We have used the neutral beam code TRANSP [16] with the module NUBEAM [17] to produce spatially resolved beam ion density distributions for actual JET pulses. Using these beam ion density distributions and the corresponding bulk ion density distributions, the neutron emission in each point on a spatial grid spanning the plasma volume has been calculated using the Monte Carlo code ControlRoom [18]. In Figure 8, three examples of neutron emission profiles are shown, calculated using this method for JET Pulse No's: 69242 (time periods 8-10s and 10.5-12.5s) and 73311 (9-10s), respectively. The two profiles from Pulse No: 69242 come from time periods where only a single Positive Ion Neutral Injector (PINI) was used at the time: on-axis PINI 4.1 and off-axis PINI 8.3, respectively. This special heating scenario gives an unsually peaked profile in the on-axis case, while it results in

a hollow profile in the off-axis case. For pulse 73311, a mixture of 14 on-and off-axis PINIs were used, giving a more smeared out emission profile.

The scattered neutron spectra as simulated using the MCNPX model with the three profiles from Figure 8 as well as with the square plasma model used in [11] as the neutron source, respectively, are shown in Figure 9.

As can be seen, the results for the hollow, peaked and smeared out profiles as well as the simple square emission source are very similar in terms of scatter spectrum shape. Also the total scatter intensities, integrated over the observed spectrum from 0.5-3.0MeV (Table 1), are close for the four cases, with the JET profiles differing less than 2% and the square less than 7%.

As can be seen (Table 1), the direct (uncollided) neutron flux is quite sensitive to the profile used in the simulation. This is due to sight line effects. The neutron emission profile may move in or out of the TOFOR field of view in the radial direction. While this will directly affect the uncollided (direct) neutron flux observed with TOFOR, it will only contribute as a secondary effect in the scattered flux, the source of which is always the far wall of the torus (divertor region), fixed relative to the TOFOR line of sight. In Table 1, also a value for the ratio between the simulated scattered and direct neutron fluxes, integrated for $E_n > 1$MeV, is given.

The small effect of the plasma profile on the scatter spectrum shape is a reassuring result for creating a scatter component for use in the analysis of TOFOR data. The smeared-out profile from JET Pulse No: 73311 was selected for use in the scatter component simulations (see section 3.5).

As discussed above and consistent with expectations, a radial displacement of the plasma seems to impact directly on the uncollided neutron flux while only marginally affecting the scattered flux. This effect was investigated in detail in a series of simulations where a narrow, homogeneous, rectangular plasma (width×height 20×100cm) was moved from the high field side to the low field side of the poloidal cross section in steps of 10-20cm along the torus midplane. The scatter spectrum result of this investigation is presented in Figure 10. Here, the MCNPX results have been multiplied with the emitting volume to allow for comparison between numbers from simulations with different source volume.

The scatter spectrum shape and intensity is similar in all cases, but the variations can be seen to be larger than when different source profiles were compared (Figure 9). To quantify the magnitude of the variations, the scatter, direct and total fluxes integrated over the energy spectrum are plotted in Figure 11 as functions of radial plasma position, normalized to their respective intensities in the simulated location furthest out on the high field side ($R = 2.6$m). It is clear that the intensity of the direct flux (short dashed red) peaks in the center of the TOFOR line-of-sight at $R = 2.6$m, while falling off to either side of the maximum as expected.

The small variations seen in the scattered flux intensity (about 9% between the extreme cases) are within the statistical error bars from the simulation. Shape variations can however be observed. In Figure 12, the scattered spectra from Figure 10 are plotted normalized to their values in the carbon scatter peak (at about 1.8MeV). An intensity variation in the nickel peak at about 2.3MeV appears in

the normalized spectrum – the relative intensities of the C and Ni peaks are clearly not constant as a function of radial position. The implication of this is that the material composition as viewed from the different angles is not the same.

It is also clear from Figure 12 that the variations in the C scatter peak are not symmetric as a function of plasma radius. The peak can be seen to cover lower energies for plasmas in the centre of the line-of-sight; the far left curve to the left of the C peak represents the central location of the source, R = 2.8-3.0m, with the following curves representing plasma positions gradually further away from the sight line centre. This could be understood in terms of equation , which shows that a scattering angle $\theta = 180^{o}$ gives the largest energy loss from the neutron to the recoil nucleus. 180^{o} scatter into the line of sight is only possible within the direct viewing cone of TOFOR, meaning the largest energy losses will only be possible in the case of a centrally located neutron source.

It should be stressed that the narrow rectangular neutron source used in this investigation was selected specifically to make observation of these subtle effects possible. The effects would not be as marked for a realistic plasma neutron source since the emission profile is wider in this case (Figure 8), spanning a larger radial section and smoothing out the effects studied. Though the effects of the radial variation on the scattered neutron flux are small, the impact on the direct flux is large as seen in Figure 11. Therefore, the scatter/direct ratios will vary as a function of radial position. It is clear from Figure 11 that the minimum ratios will be obtained when a maximal fraction of the direct flux is emitted within the field of view of the detecting instrument, while larger ratios will be obtained for plasmas displaced to either side of the LOS. The numerical values of scatter/direct obtained from these simulations will not be directly comparable with TOFOR measurements due to the unique shape of the plasma source (20×100 cm).

The effects of radial and vertical shifts in plasma position on the expected scattered flux were discussed also in ref [9], where it was concluded that a radial shift affected the scatter intensity while a vertical shift did not. Since the viewing geometry was horizontal in the simulations for that paper while vertical in our case, our radial result of little impact on the scatter component should be consistent with the vertical result in ref [9], which is also observed.

3.4. EFFECT OF VERTICAL DISPLACEMENTS

For completeness, also the effect of moving the neutron source in the vertical direction has been studied. In this case, a small, square source (width×height 20×20cm), located between 280 and 300cm major radius, was used. The source was moved in the vertical direction in increments of 10cm from −20 to +30 cm relative to the torus midplane. The result is shown in Figure 13.

The effects of these small movements on the scatter component are minor. However, if the integrated fluxes are normalized to their values at the $Z = -20$ cm extreme, a clearly decreasing trend is seen for the scatter intensity as the neutron source is moved in the positive direction, i.e., further from the wall responsible for the scatter and closer to the detecting instrument (Figure 14). The opposite effect, though small for the limited displacements studied here, can also be

observed for the direct flux.

This is in agreement with the results obtained in [9] concerning radial displacements, though the effects observed here are smaller since the displacements studied are smaller relative to the total distances involved in the configuration far wall - neutron source - detecting instrument in these calculations. The deduced scatter/direct ratio ($E_n > 1$MeV) varies from 0.071 to 0.057 between the two extremes in our simulation, i.e., a relative drop of about 20%. Note, however, that due to the unrealistic shape of the plasma source in this case (20×20cm), the results obtained are not comparable with real TOFOR data.

3.5. SIMULATED SCATTER MATRIX FOR USE IN THE TOFOR DATA ANALYSIS

Scattered neutron spectra have been simulated for quasi-monoenergetic (±25 keV) neutron sources in the interval 1 to 18MeV in steps of 50keV, using the smeared out neutron emission profile from the TRANSP simulation for JET Pulse No: 73311 (Figure 8c) and the material composition for the divertor region obtained from the drawing office (section 3.1). The result is a scatter matrix with resulting scatter spectra for each source energy (Figure 15).

Examples of simulated scattered neutron spectra for 2.5±0.025 and 14.0±0.025MeV neutron sources are shown in Figure 16. The number of source neutrons simulated is 50×106 independent on incident neutron energy; a larger number of simulated neutrons would reduce the statistical error (represented with error bars in Figure 16).

The scatter matrix in Figure 15 is used to create a scatter component for use in the TOFOR data analysis by folding the matrix with an estimate of the neutron emission spectrum from a preliminary fit to the data, as will be further discussed in section 4. The scatter matrix is produced with bins of 50keV width to match the resolution of the TOFOR response function.

The simulation studies discussed above show that the impact of the neutron emission profile, radial and vertical positions on the *shape* of the scattered neutron spectrum is small. We are confident that use of the neutron emission profile for Pulse No: 73311 in the generation of the scatter matrix introduces only minor additional uncertainties in the extracted physics results.

It should be emphasized that with this method, the scattered neutron component for use in the data analysis is determined based on the measured neutron emission spectroscopy data only. In [9], it is anticipated that for detailed subtraction of the scatter, the temperature of a plasma (assumed to be thermonuclear) needs to be known. Our results show that this is not necessary.

The fraction of scattered neutrons relative to direct will vary with the simulated neutron energy for two reasons. Firstly, the cross sections of elastic neutron scattering vary with energy, giving an intensity variation for different simulated source energies. Secondly, the fraction of the scatter spectrum with $E_n > 1$MeV measureable with TOFOR increases with increasing source neutron energy. As an example, the fraction of scattered-to-direct neutrons observable with TOFOR for the $E_n = 2.5$MeV simulation is 0.174±0.005, while the average simulated scatter/direct ratio from 2.2-2.8MeV is 0.185±0.005. This means that a scatter/direct comparison between measured and

simulated data needs to take the neutron emission energy spectrum into account.

4. RESULTS OF EXPERIMENTS

In this section, the scatter results from the MCNPX simulations are compared with measured TOFOR data. As described in section 2, the shape of the measured t_{TOF} spectrum in the region of low E_n (or, equivalently, high t_{TOF}) is crucially dependent on discriminator thresholds set in the data acquisition electronics. Because of this, only pulses from the interval 71650-74000 with well-known threshold settings and, hence, well-defined response function (with estimated uncertainty as in Figure 1 and Figure 2) are studied here.

As a general consistency check between model and data, a neutron spectrum as measured with TOFOR (points with error bars) is compared with the total simulated neutron energy spectrum obtained from MCNPX (solid blue line) in Figure 17. The t_{TOF} spectrum shows summed TOFOR data from plasma periods from JET pulses in the interval 71650-74000 with no auxiliary heating applied (ohmic plasmas). The thermonuclear neutron emission from such ohmic plasmas describes a narrow, nearly Gaussian energy spectrum with a broadening directly related to the bulk ion temperature as derived in [19]. The fitted component in Figure 17 is simulated using such a deuterium plasma source with $T_d = 2.7$keV in MCNPX. A couple of observations can be made about the result. The measured direct spectrum is nicely reproduced in the simulation assuming $T_d = 2.7$ keV (main peak at $t_{TOF} = 65$ ns). The relative contribution of direct and scattered neutrons (ratio of peak-to-high t_{TOF} side) is approximately right. There is some discrepancy in the shape of the scatter between the measurement and the simulation. Two factors come into play here. Firstly, the uncertainty in the response function affects the ability to accurately describe the measured events at higher t_{TOF} with a simulated component. Secondly, as indicated in the discussion about the effect of the assumed material composition in section 3.1, a higher fraction of Ni relative to C in the model would increase the scatter contribution on the high t_{TOF} side of the main peak, while decreasing the contribution in the C peak around 75ns, likely improving the match between model and data. This is an indication that the material information as included in the MCNPX model might indeed not perfectly describe the divertor region.

In the more complex case of applied auxiliary heating, MCNPX has not been used to predict the shape of the emitted (direct) neutron energy spectrum. Instead, it is obtained from TOFOR data. Data are analyzed by constructing a set of components, describing the neutron emission from reactions between different ion populations present in the plasma, and fitting the parameterized components to the data using the method suggested by Cash [20], i.e., minimization of the metric

$$C = 2 \sum_{j=1}^{n_l} (x_i - x_i \ln x_i) \tag{2}$$

where x_i is the value of the fitted parameter and n_i the number of counts in each bin. A reduced value of the metric, C_{red}, is obtained by dividing by u-p, where u is the number of bins and p the

number of free parameters in the fit. As in the case of reduced χ^2, C_{red} should on average also tend to unity for a good fit. Note that also the randoms background, though subtracted in the figures, is treated as a parameter in the fit.

TOFOR was built to measure the (t_{TOF} manifestation) of the neutron energy spectrum. However, the measured data will be a superposition of direct and scattered neutrons. TOFOR analysis taking scattered neutrons into account is done by (i) estimating the direct spectrum through a preliminary fit without taking scattered neutrons into account (ii) folding this direct spectrum with the scatter matrix obtained as described in section 3.5 (iii) fitting with the preliminary scatter component to obtain a better estimate of the direct spectrum and iterating, repeating the process until a good description of the data is obtained. This method was used also in the preliminary work in [11].

Pulses with Neutral Beam (NB) heating ($P_{NB} > 10$MW) and no Radio Frequency (RF) heating from the pulse range 71650-74000 are selected to get a data set with good statistics and similar features to test the scatter component. The direct emission is assumed to consist of three components, describing reactions between two ions from the thermal bulk population, beam-thermal reactions and beam-beam ion reactions, respectively. The thermal component is parameterized as a Gaussian with intensity and width ($\sigma = 35.0 \cdot \sqrt{T}$d keV, with T_d in keV) as free parameters and the beam-thermal as a uniform distribution in ion energy space with the maximum energy and intensity as free parameters. The shape of the beam-beam component is created from the TRANSP beam distribution output from Pulse No: 73311, using ControlRoom to determine the neutron spectrum when the beam distribution reacts with itself. In this case, only the intensity is left as a free parameter.

Figure 18a shows the C_{red} results from fitting the three direct components only to TOFOR data for the set of NB heated pulses. The mean is $C_{red} = 12.5$, with a standard deviation of 5.3. If the scatter component is taken into account using the method outlined above, the result in Figure 18b is instead obtained, with average $C_{red} = 1.1$ and standard deviation 0.30. It is clear that the scatter component is needed to describe the data.

Examples of fits to TOFOR data for JET Pulse No's: 73183, 73311 and 73703 from the set of NB heated pulses are shown in Figure 19. *C*red in the three cases is 2.03, 0.98 and 0.99, respectively. Also shown in Figure 19 are the representations of the components on the *E*n scale. As can be seen, the thermal emission dominates for Pulse No: 73183, the beam-beam emission is strong for pulse 73311 and the beam-thermal dominates for Pulse No: 73703, leading to different shapes of the direct spectra with a corresponding perceivable impact on the shape of the scattered spectra.

In Figure 20a, the data from all NB heated pulses with P_{NB}>10MeV in the interval selected for study are summed to obtain a t_{TOF} spectrum with statistics sufficiently high for analysis also in the region of 14MeV neutrons (~27ns). The 14 MeV neutron peak in this data set is due to reactions between bulk deuterium and the tritium from d+d→t+p reactions, i.e., Triton Burn-up Neutrons (TBN). The TBN component shape is simulated using ControlRoom; only the intensity is left as a free parameter in the fit. For simplicity, and since it would not affect the spectrum below $t_{TOF} = 55$ns, the beam-beam component is excluded here. Figure 20 shows that the thermal, beam-

thermal, TBN and scatter components can be invoked to nicely describe the measured neutron spectrum from E_n = 1-18MeV, with the neutron energy representation illustrated in panel (b). Even the structure due to the first excited state of 12C (Figure 16b) can be discerned in the measured data (around t_{TOF} = 40ns).

As discussed in section 3, the intensity of the direct neutron flux reaching TOFOR should depend on plasma profile and position while the scattered flux intensity to lowest order should not. This could be checked by comparing scatter and direct intensities from the fits to the set of TOFOR data from NB heated pulses with $P_{NB} > 10$MW with the total neutron yield during the plasma periods studied as measured with the JET fission chambers (KN1). Such a comparison is done in Figure 21a (scatter) and b (direct), showing also linear fits to the data (solid red lines). The spread in the two cases is quantified through introducing a goodness of fit metric G according to averaged over 253 points (one per pulse) in each plot. It is clear that a lower value of G means a smaller average deviation from the line in the fit. There is a larger spread for direct/KN1 (G = 0.68) compared to scatter/KN1 (G = 0.12), consistent with the hypothesis that the direct flux is profile and position dependent while the scattered flux is not.

$$G = \left\langle \frac{|y_i - l|}{\sigma_i} \right\rangle \tag{3}$$

The average ratio scatter/KN1 is 4.6×10^{-11} and direct/KN1 2.4×10^{-10}. The small spread in the scatter case justifies normalization of the scatter intensity relative to KN1 to reduce the uncertainty of the fit for pulses with lower neutron emission and hence lower statistics in the TOFOR data.

4.1 COMPARISON OF EXPERIMENT AND SIMULATION RESULTS

It is interesting to compare the scatter/direct ratios obtained from analysis of experimental data with those obtained from the simulations as a quantifiable benchmark of the goodness of the modeling. When obtaining the numbers for such a comparison, it is of course essential to integrate the scatter over the same interval from simulations and measurements. Here, we select a lower cut-off in the integration of E_n = 1MeV, since no experimental observation of the energy spectrum below this cut-off is possible (Figure 2).

Figure 22 shows the scatter/direct ratio from analysis of TOFOR experimental data as a function of pulse number for the set of similar NB heated pulses described above. Also shown is a zero-degree polynomial fit to the data, giving a scatter/direct average of 0.187 (G=0.14) for the set of pulses included.

This can be compared with the corresponding value given by the MCNPX modeling. Neutron spectra from NB heated JET plasmas (with injection energies E_{NB} in the range 80-130keV) can be approximated with flat distributions in the range 2.2–2.8MeV. The average of simulated scatter/direct ratios (E_n = ≥1MeV) for source energies E_n = 2.2–2.8MeV is 0.185 (statistical error 0.005), to be compared with the average ratio from analysis of experimental data of 0.187. As discussed

above (section 3.5), the scatter intensity will be dependent on the energy of the source neutrons. The magnitude of the effect in this case has been checked by folding the scatter and direct matrices from MCNPX with the direct spectra obtained from TOFOR analysis, integrating and taking the ratios. The result is illustrated in Figure 23, where the obtained scatter/direct ratios are shown as functions of pulse number. As can be seen, the spread due to source spectrum shape variations is very small indeed, with values ranging from 0.181-0.187. The average is 0.185 and the standard deviation 0.001 assuming the values are Gaussian distributed in scatter/direct space; this is however not quite the case as can be seen from the frequency distribution to the right in Figure 23.

The agreement between scatter/direct from measurements of 0.187 and simulations of 0.185 is remarkable. However, the numbers are subject to a number of uncertainties. Systematic uncertainties are introduced due to the line-of-sight implementation and the material composition selected for use in the model. No attempt is made to quantify these uncertainties, but the statistical MCNPX uncertainty of 0.005 is likely negligible in the context. The main systematic uncertainty in the data analysis is the discriminator thresholds of TOFOR. This effect is quantifiable: redoing the analysis of measured data using response functions with the upper and lower extreme values of the threshold settings within the uncertainty interval (see section 2) gives scatter/direct ratios of 0.134 and 0.232 with mean C_{red} of 1.2 and 1.5, respectively. It should be noted that these values represent the extremes; it is not likely that the thresholds for all 37 TOFOR detector channels systematically deviate ΔE_p = 60keV from the target values of 380keV.

A number of uncertainties also affect the obtained result on a pulse-to-pulse basis. The effect of the shape of the direct E_n spectrum has already been discussed (Figure 23) and found to be small. As discussed in section 3, also the location of the plasma and the plasma profile will play a role. The MCNPX result is obtained using the profile for JET Pulse No: 73311. The spread in plasma profiles and positions was limited by selecting similar NB heated pulses with high neutron emission in the analysis. However, data on the location of the magnetic axis in the radial and vertical directions can be extracted from the JET database for each of the pulses studied. In Figure 24, the scatter/direct ratios from Figure 23 are plotted as functions of radial magnetic axis location (R_{mag}), and in Figure 25 as a function of vertical (Z_{mag}). For JET Pulse No:73311, Rmag=3.09 m and Z_{mag} = 3.05m.

No strong trends in the plotted scatter/direct values are observed as functions of R_{mag} or Z_{mag} - the spread in scatter/direct is in both cases much larger than the, possible, small dependence on R_{mag} or Z_{mag}. Also shown in Figure 24 and Figure 25 are fits to the data (solid red lines) with slope 0.03 m-1 in the Rmag case (G=0.14) and -0.02m^{-1} in the Z_{mag} case (G=0.14). These slopes, if significant, would give position-dependent variations in scatter/direct of 0.005 over the 2.96-3.14m in the radial case, and 0.007 over the 0.04-0.41m in the vertical case. It should be noted that the fitted slopes are consistent with the simulations in sections 3.3 and 3.4, which showed that the scatter/direct ratio should increase with R in this region (R>2.9m) in the radial case, and decrease with Z in the vertical case.

5. DISCUSSION

In summary, it has been shown that the MCNPX simulation scatter results are consistent with the results from analysis of TOFOR measurements. Variations in neutron source shape, vertical and horizontal position are shown to have a small impact on the shape and intensity of the scattered neutron spectrum in the TOFOR line-of-sight, but a larger impact on the direct flux. The material composition used in the MCNPX model will have a direct impact on the shape of the scatter component. This means that it is essential to make every effort to obtain a good description of the vessel wall constituents on a nuclide level. It also means that the shape of the scattered spectrum will be dependent on viewing geometry; a horizontal radial view at JET, for instance, would not include scattered neutrons from the divertor region but from the inner vessel wall with a quite different material composition. Finally, it also means that any changes in the vessel design will require new simulations to determine the corresponding new scatter matrix for use in the data analysis.

Such a vessel design change is currently being undertaken at JET with the installation of the ITER Like Wall (ILW). The planned composition of the plasma-facing materials after the upgrade is discussed in [21]. Specifically in the divertor region, the central Carbon Fibre Composite (CFC) tile will be replaced with a bulk tungsten tile, and the surrounding CFC tiles coated with a 200mm thick layer of tungsten. A quick test of the impact of these structural changes on the scatter spectrum was done by replacing the central CFC tile with a W tile in the model, neglecting the W coating of the other tiles and the detailed structure of the bulk W tile. In Figure 26, the result from this test (solid red) is compared with the result from our model of the current JET setup (dashed blue), for MCNPX runs with quasi-monoenergetic 2.5MeV neutrons. As can be seen, the relative contributions from the C and Ni peaks change.

The magnitude of the scattered flux has important implications for the possibility of using neutron spectrometry as a tool for determining the fuel ion density ratio, n_t/n_d, for future reactors such as ITER, because of its implications for the feasibility of distinguishing the 2.5MeV neutron peak from the background of 14MeV backscatter. The crucial point here is the signal (2.5MeV DD neutron peak amplitude) to background (14MeV DT scatter amplitude) ratio in the neutron energy region around 2.5MeV, which will determine whether accurate information about the 2.5MeV DD neutron flux can be obtained. The model described in this paper has been used to predict the signal-to-background ratio in the TOFOR line-of-sight at JET for ohmic 2.5 and 20keV DT plasmas (Figure 27). The prediction relies on an assumption of the relative DT and DD neutron rates, Y_{DT}/Y_{DD}; assuming a DT plasma with 50% D/T (i.e., $n_d = n_t$), this ratio is 210 for a 2.5keV plasma and 330 for a 20keV plasma. This gives signal-to-background ratios of about 2.1 in the 2.5keV case and 1.2 in the 20keV case.

Diverging predictions on this signal-to-background ratio at ITER can be found in the literature (see e.g. [3,4,5,6,7,9]). In this paper, we have seen that dedicated simulations taking into account the specific line-of-sight information for a planned instrument would be needed in order to accurately predict the measurement conditions. Two main factors will affect the result:

- The material composition will have a crucial effect on the shape of the scattered neutron

spectrum. Any detailed predictions on the signal-to-background ratio in the region of the 2.5MeV DD neutron peak at ITER must include an estimate of the expected nuclide composition of the wall.

- The assumed viewing geometry will have an impact; we have found here that the relative distances scattering wall – neutron source – detecting instrument affect the simulated scatter/direct ratios (section 3.4).

CONCLUSIONS

In this paper, a method of including scattered neutrons in the analysis of neutron spectral data without prior knowledge of the plasma source properties is established. A scatter matrix is simulated with scatter spectra as a function of source neutron energy; this matrix is folded with the direct neutron spectrum for each pulse studied to obtain a plasma-specific scatter component for use in the analysis. Simulations show that the shape and magnitude of the scattered spectrum in the TOFOR line-of-sight is only marginally affected by plasma shape and position. This means that the same scatter matrix can be used with confidence in the analysis of TOFOR data from most JET plasma scenarios.

It is shown that the scatter component obtained in this way is essential in describing the measured TOFOR data. Inclusion of the component in analysis of some 250NB heated JET pulses gives an average goodness of fit value $C_{red} = 1.1 \pm 0.3$, while fits that do not take scatter into account give $C_{red} = 12.5 \pm 5.3$.

The scattered neutron intensity as observed with TOFOR is found to be more closely related than the direct intensity to the total neutron yield as measured with the JET fission chambers, consistent with the expectation from simulations. The small spread in TOFOR scatter intensity relative to the total neutron yield motivates fixing of this parameter in the analysis relative to the JET fission chambers to improve the accuracy for pulses with lower statistics.

The material composition of the scattering wall is identified as crucial in modelling of the expected scattered flux. It is also clear that the viewing geometry will have an impact on the relative intensity of scattered and direct neutrons. This means that a dedicated individual determination of the scattered neutron flux is necessary for each relevant instrument location.

Any simulation model based on engineering drawings will include uncertainties in the material composition on an isotope level. It would be interesting to be able to measure the detailed shape of the scattered spectrum, in an energy region with no direct neutron flux. In the case of TOFOR, the instrument response with multiscattered neutrons interfering in the region of energy-degraded scattered neutrons from the vessel makes such detailed measurements of the scattered flux difficult, even though TOFOR has the energy bite required both in the 2.5 and 14MeV cases. However, we show that the scatter spectrum shape obtained from MCNPX simulations in this paper describes the scattered flux sufficiently well over the full energy range 1–18MeV.

The excellent agreement between simulations and measurements found in terms of scatter/direct ratios, with 18.5±0.5% from the simulations and 18.7±5.0% from measurements, serves as a solid

benchmark of the MCNPX model used. Also a small drop in scatter/direct with vertical plasma source displacements and a small increase with radial displacements are observed in the measurements, consistent with the predictions from simulations.

ACKNOWLEDGEMENTS

This work, supported by the European Communities under the contract of Association between EURATOM and VR, was carried out under the framework of the European Fusion Development Agreement. The views and opinions expressed herein do not necessarily reflect those of the European Commission. The authors gratefully acknowledge all the help from Paul Carman at the JET drawing office in obtaining data about the material composition in the TOFOR line of sight. The computations were performed on UPPMAX resources under Project p2007016.

REFERENCES

[1]. Jarvis O.N. 1994 *Plasma Physics and Controlled Fusion* **36** 209-244

[2]. von Goeler S, Johnson L.C, Bitter M, Efthimion P.C. and Roquemore A.L. 1997 *Rev Sci Inst* **68** (1)

[3]. Källne J, Batistoni P. and Gorini G. 1991 *Rev Sci Inst* **62** no 12 2871

[4]. Marocco D, Belli F, Bonheure G, Esposito B, Haschuck Y, Petrizzi L and Riva M 2007 The ITER Radial Neutron Camera Detection System *Proceedings of the International Workshop on Burning Plasma Diagnostics, Varenna, Italy, 24th-28th September 2007 AIP conference proceedings* Vol. 988, p. 291

[5]. Petrizzi L *et al* 2007 *Fusion Engineering and Design* **82** 1308-1314

[6]. Moro F, Petrizzi L, Brolatti G, Esposito B, Marocco D and Villari R 2009 *Fusion Engineering and Design* **84** 1351-1356

[7]. Okada K, Kondo K, Sato S, Nishitani T, Nomura. K, Okamoto A, Iwasaki T, Kitajima S and Sasao M 2006 *Review of Scientific Instruments* **77** 10E726

[8]. Krása J *et al* 2008 Plasma Physics and Controlled Fusion **50** 125006 (10pp)

[9]. Antozzi P, Gorini G, Källne J and Ramström E 1996 *Nucl Instr and Meth A* **368** 457-472

[10]. M. Gatu Johnson *et al* 2008 *Nucl Instr and Meth A* **591** 417-430

[11]. M. Gatu Johnson *et al* 2007 The TOFOR neutron spectrometer for high-performance measurements of D plasma fuel ion properties *Proceedings from the International Workshop on Burning Plasma Diagnostics, Varenna, Italy, 24th-28th Sept 2007 AIP conference proceedings* Vol. 988, p. 311

[12]. MCNPX Version 2.5.0 User's Manual * (LA-CP-05-0369, April 2005) https://mcnpx.lanl.gov/

[13]. Hjalmarsson A, Conroy S, Ericsson G, Giacomelli L and Källne J 2006 Response function simulations of the TOFOR neutron time-of-flight spectrometer *Uppsala University Neutron Physics Report UU-NF 06#06 (September 2006)*

[14]. Gherendi M *et al* 2008 *Journal of Optoelectronics and Advanced Materials* **10** 2092-2094

[15]. Knoll G.F. 2000 Radiation Detection and Measurement 3rd Ed., John Viley and Sons, Inc.
[16]. Ongena J *et al* 2006 Transactions of Fusion Science and Technology **49** 337-345
[17]. Pankin A, McCune D, Andre R, Bateman G. and Kritz A., 2004 Computer Physics Communications **159** 157–184
[18]. Ballabio L 2003 *Calculation and Measurement of the Neutron Emission Spectrum due to Thermonuclear and Higher-Order Reactions in Tokamak Plasmas PhD Thesis, Acta Universitatis Upsaliensis No. 797* Faculty of Science and Technology Uppsala University
[19]. Lehner G. and Pohl F 1967 Zeitschrift für Physik **207** 83-104
[20]. Cash W. 1979 *Astrophys* J **228** 939-947
[21]. Matthews G.F., *et al* 2007 *Physica Scripta* **T128** 137-143

	Scatter, $E_n \geq 0.5$MeV	**Scatter, $E_n \geq 1$MeV**	**Direct**	**Total**	**Scatter/direct**
Hollow	1.02×10^{-11}	6.11×10^{-12}	3.72×10^{-11}	4.73×10^{-11}	0.164±0.003
Peaked	1.03×10^{-11}	6.18×10^{-12}	5.08×10^{-11}	6.11×10^{-11}	0.121±0.003
Smeared	1.01×10^{-11}	5.96×10^{-12}	3.44×10^{-11}	4.45×10^{-11}	0.173±0.003
1 m^2	1.08×10^{-11}	6.52×10^{-12}	3.61×10^{-11}	4.68×10^{-11}	0.181±0.003

Table 1. Scattered, direct and total neutron intensities at the location of TOFOR as simulated using MCNPX with hollow, peaked, smeared and square neutron emission profiles as described in the text. The scattered intensity is given both as a total ($E_n \geq 0.5$MeV, column 2) and a value that is suitable for comparison with TOFOR data ($E_n \geq 1$ MeV, column 3). Also the estimated ratio of scatter/direct, based on the 3rd and 4th columns, is given (right column). The intensities are given in units of [neutron^{-1}].

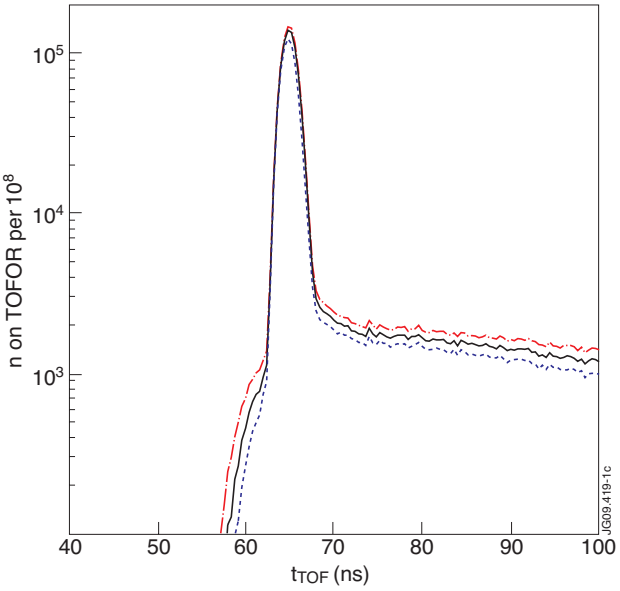

Figure 1: TOFOR response to quasi mono-energetic 2.45±0.025MeV neutrons as simulated using GEANT4. The curves represent the target discriminator threshold settings (E_p=380keV, solid black) and the extremes within the estimated threshold uncertainty (dash-dot red for E_p =320keV, dashed blue for E_p = 440keV).

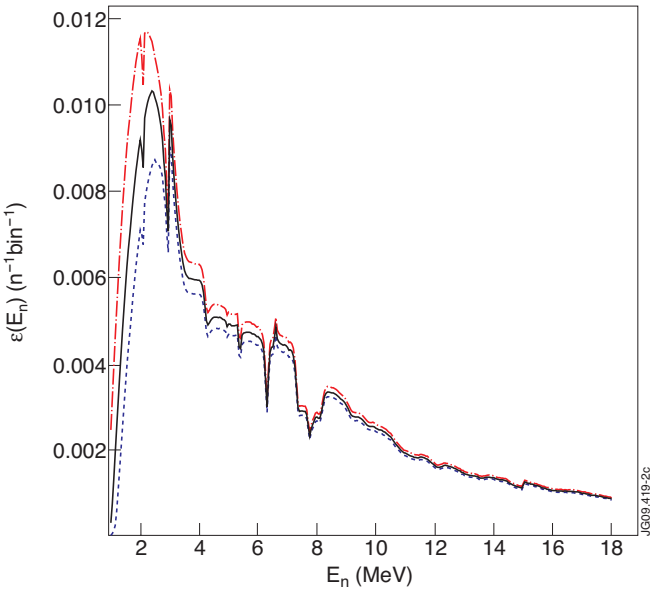

Figure 2: TOFOR efficiency as a function of incident neutron energy, E_n, determined through integrating the flight time spectrum (as in Figure 1) for each simulated energy, for the target threshold settings and the extremes within the uncertainty (colours as in Figure 1).

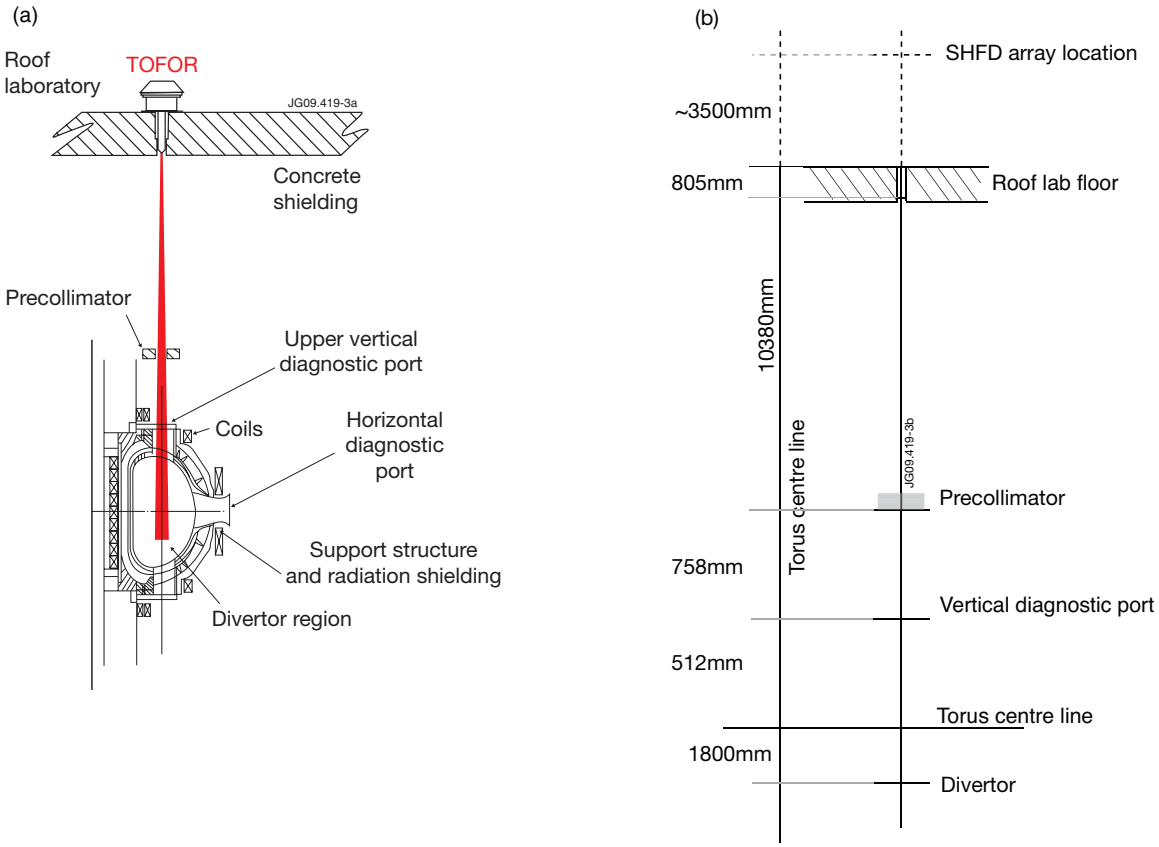

Figure 3: (a) The vertical TOFOR line-of-sight through the JET vessel, defined by the collimator through the roof laboratory floor, the precollimator structure and the upper vertical port. (b) Vertical distances between relevant structures in the TOFOR line-of-sight.

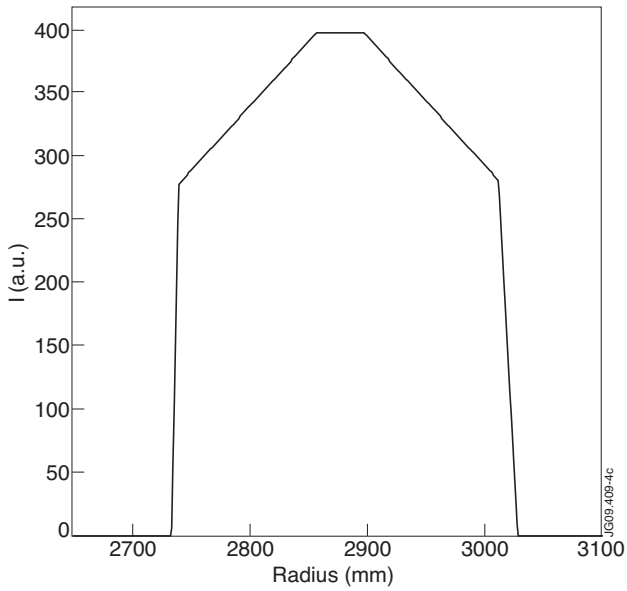

Figure 4: TOFOR field of view at the torus midplane as calculated in the radial plane only (assuming a symmetric line-of-sight in the toroidal direction). The 4cm of "full" view around 2.88m correspond to the diameter of the roof laboratory floor collimator and the primary TOFOR detector.

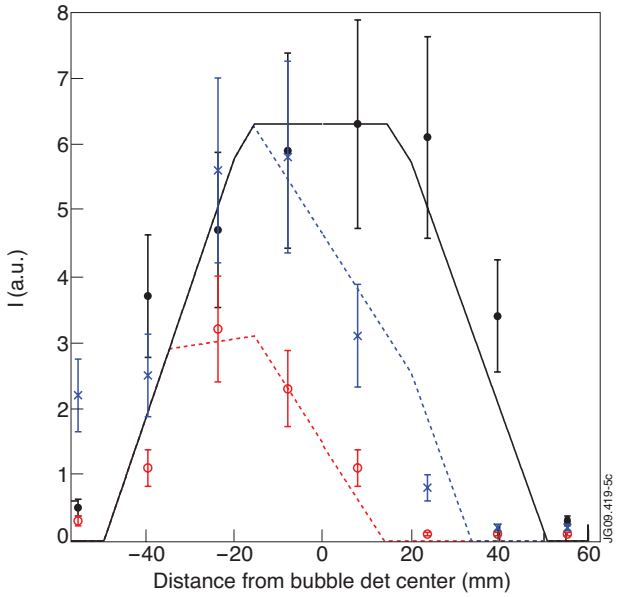

Figure 5: Calculated (lines) and measured (points with error bars) footprints at a location 3.5m above TOFOR in the JET roof laboratory. The three curves represent the expected footprint from an assumed plasma with a flat neutron emission profile in the line-of-sight with a fully open outer precollimator jaw (solid black), a jaw set to 82.7mm (short dashed blue) and one set to 22.7mm (long dashed red), respectively. The points represent SHFD measurements for Pulse No's: 73746 with open precollimator (black circles), 73751 set to 22.7mm (red hollow circles) and 73754 set to 82.7mm (blue crosses).

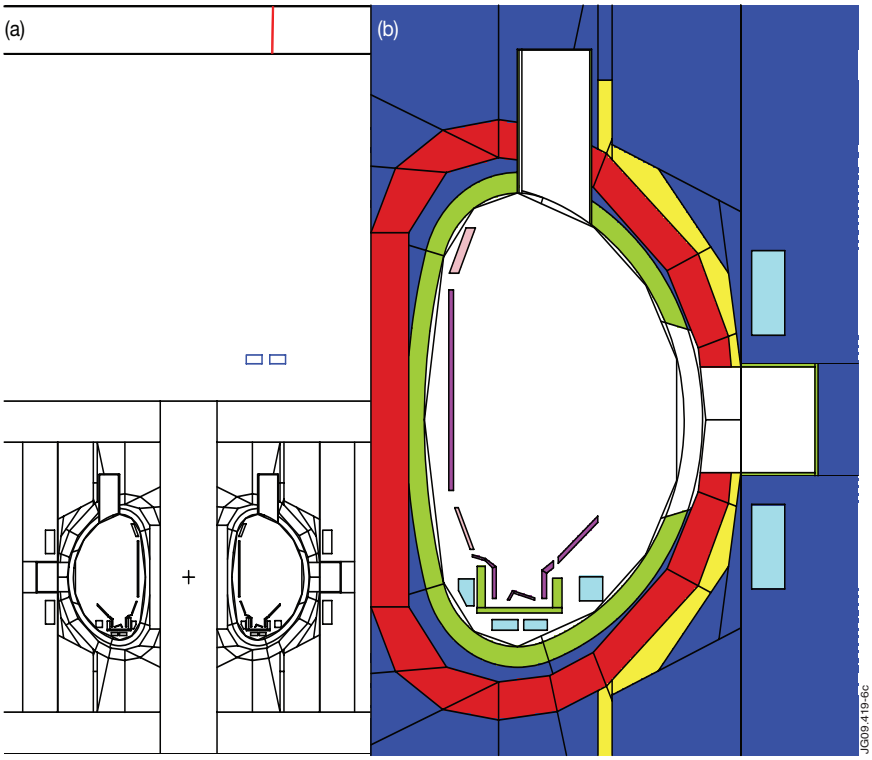

Figure 6: Visualization of the JET MCNPX model used in the backscatter simulations, showing (a) the cross section of the JET torus, the precollimator structure (blue) and the collimator through the roof laboratory floor (red) (compare Figure 3) and (b) a detailed view of the JET torus, indicating,

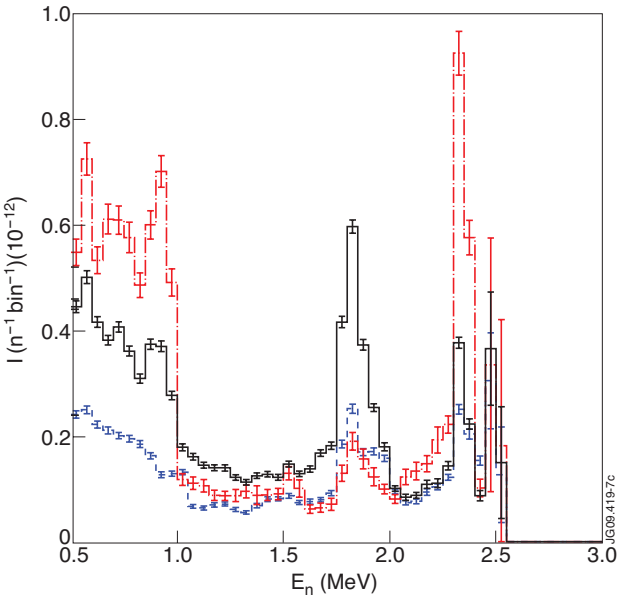

Figure 7: Scattered neutron spectra from MCNPX, per cm^2 on the primary TOFOR detector, using the model described in [11] (short dashed blue), the new model used in this paper (solid black) and a version of the new model with a higher contribution of Ni relative to C (dash-dot red). The error bars show the statistical error from the simulation. The MCNPX output is given per simulated neutron. e.g., the level of detail included in the modelling of the divertor and the vertical port. The different colours in (b) indicate different material compositions.

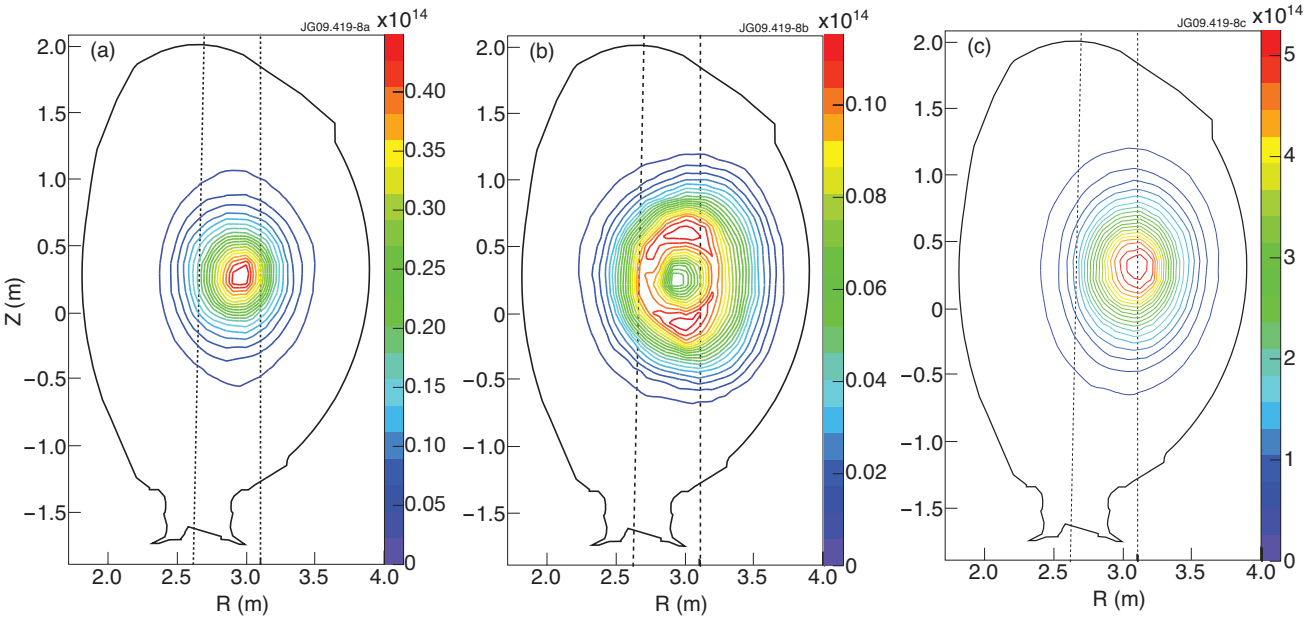

Figure 8: Neutron emission profiles calculated based on the fast ion density profile output from the TRANSP module NUBEAM as described in the text for JET Pulse No's: (a) 69242 8-10s (peaked), (b) 69242 10.5-12.5s (hollow) and (c) 73311 9-10s. The two vertical lines approximately indicate the extent of the TOFOR LOS.

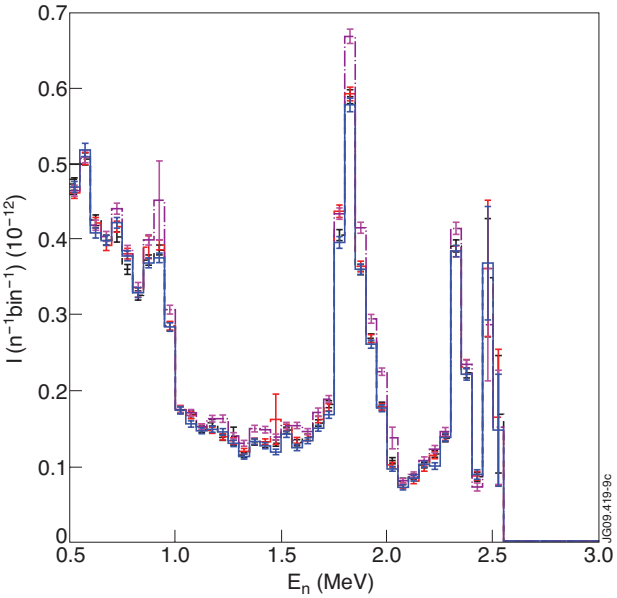

Figure 9: Scattered neutron spectra per cm^2 on the primary TOFOR detector, simulated using MCNPX for the hollow (black) and peaked (red) neutron emission profiles from JET Pulse No: 69242, the smeared profile from Pulse No: 73311 (blue) and the 1m^2 square neutron source used in ref [11] (magenta), respectively.

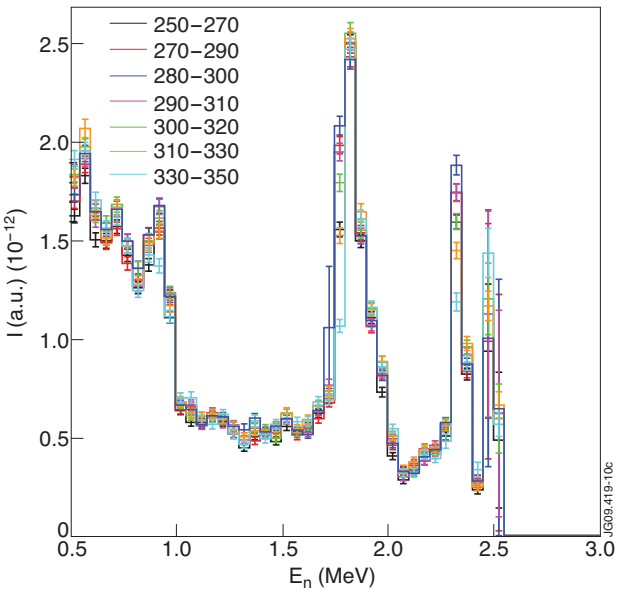

Figure 10 Scattered neutron spectra per cm^2 on the primary TOFOR detector, simulated using MCNPX with a narrow rectangular plasma source moved from the high-field side (250-270cm) towards the low field side (330-350cm) in steps of 10-20cm as indicated by the legend. The MCNPX output (in units of n^{-1} bin^{-1}) has been multiplied with the emitting volume to give a comparable emissivity in the TOFOR LOS for the seven cases.

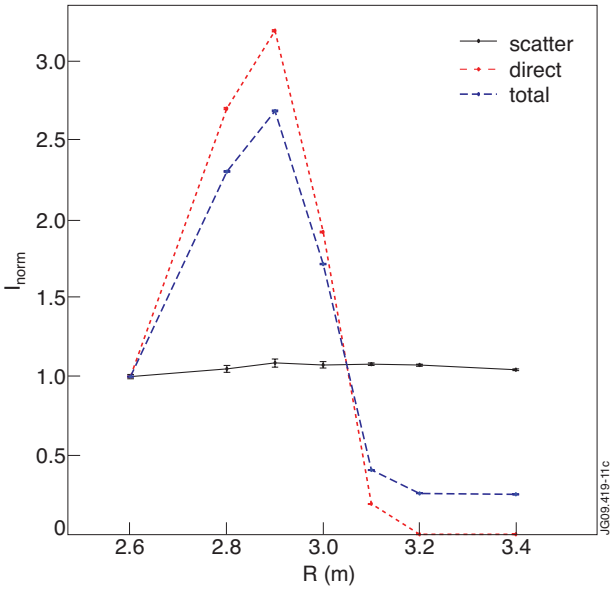

Figure 11: Variations in scatter (solid black), direct (short dashed red) and total (long dashed blue) intensities as simulated with MCNPX as a function of position along the JET major radius. The intensities are normalized to their values at R=2.6m.

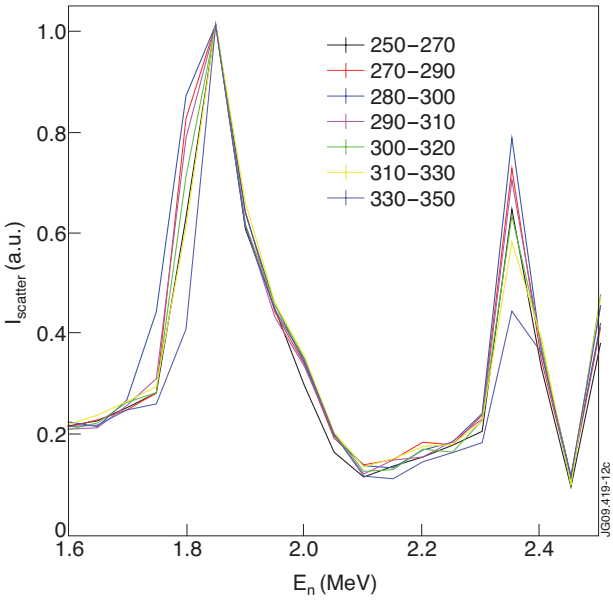

Figure 12: Scattered neutron spectra as in Figure 10 normalized to their values in the C scatter peak. The curves represent lines between the center points of the histogram bins.

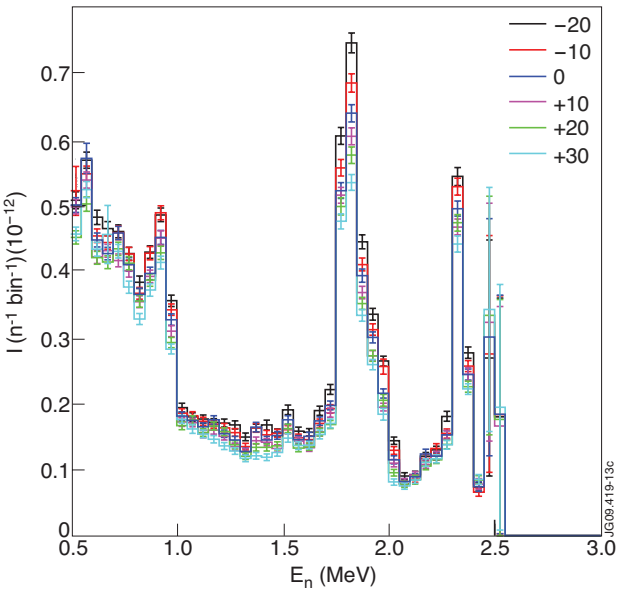

Figure 13: Scattered neutron spectra, per cm^2 on the primary TOFOR detector, simulated with MCNPX using a 20×20cm square neutron source, for vertical positions −20 to +30cm relative to the torus midplane as indicated in the label.

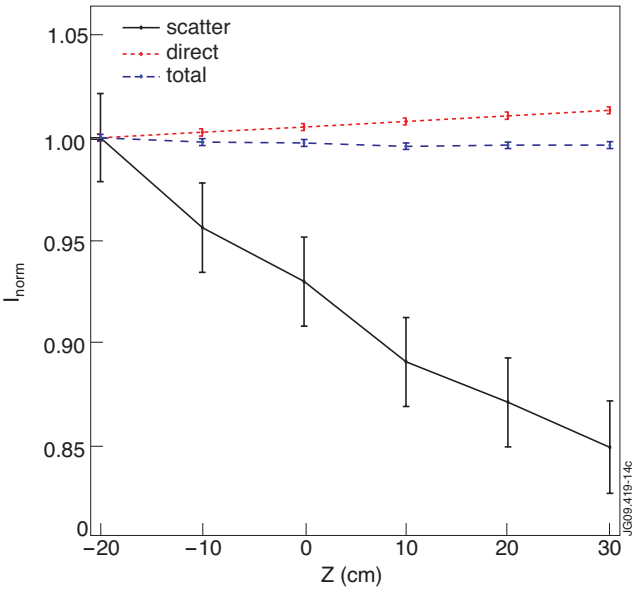

Figure 14: Relative intensities for scatter (solid black), direct (short dashed red) and total (long dashed blue) neutron fluxes from MCNPX, each normalized to their values in the Z=−20 cm point.

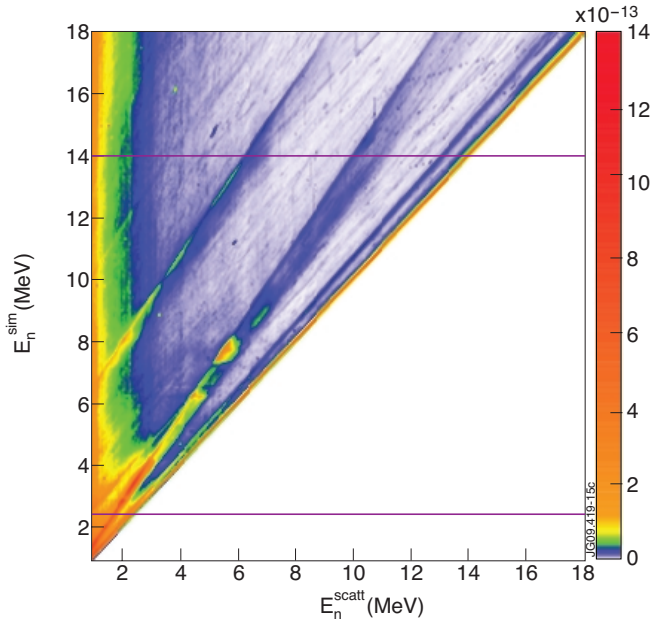

Figure 15: Matrix of simulated scattered neutron spectra (x axis) for simulated source neutron energies from 1 to 18MeV (y axis). The lines (magenta) indicate the simulated neutron energies E_n=2.5 and 14MeV, respectively; the corresponding simulated scatter spectra are visualized in Figure 16.The diagonal bands of higher intensity represent inscatter and scatter on Ni and C nuclei, as indicated in Figure 16.

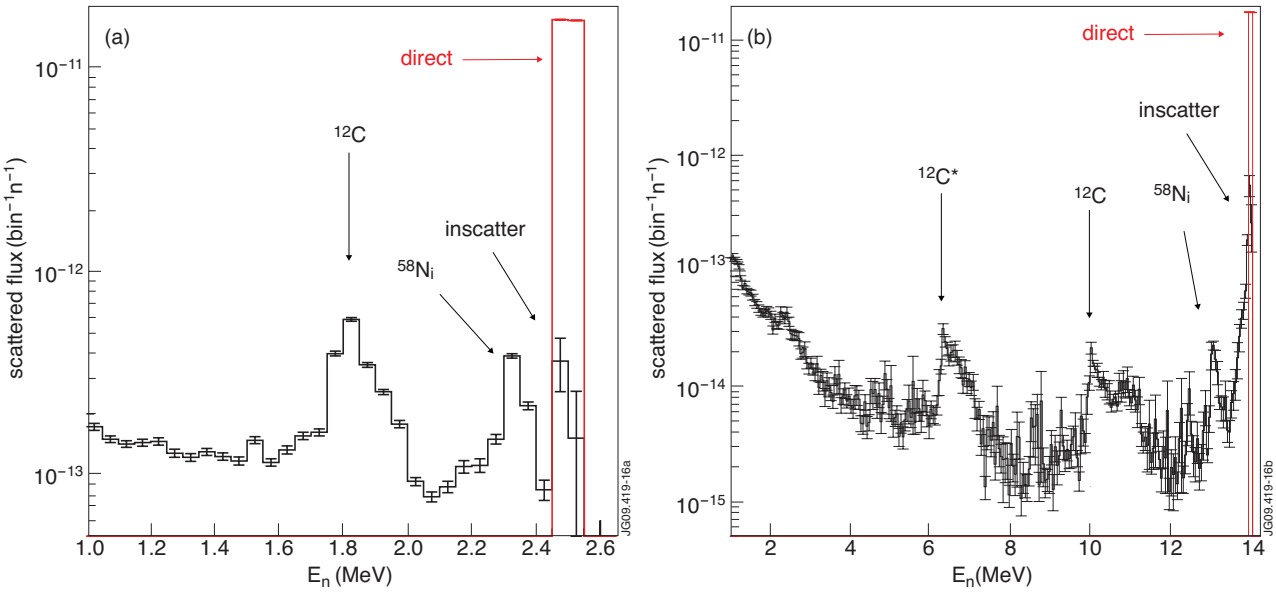

Figure 16. Simulated scattered neutron spectra per cm^2 on the primary TOFOR detector for source neutron energies (a) E_n=2.5±0.025MeV and (b) E_n=14.0±0.025MeV (solid black), with the main carbon, nickel and inscatter peaks indicated (corresponding to bands of higher intensity in Figure 15). Also shown are the corresponding simulated direct neutron spectra (dashed red).

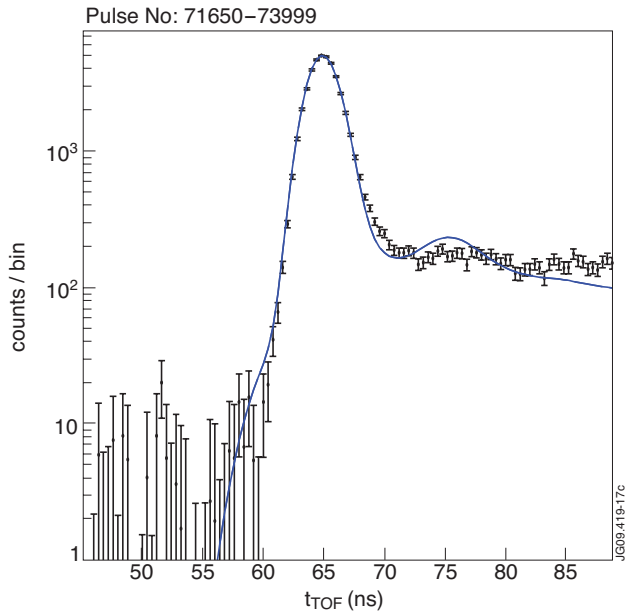

Figure 17. Summed TOFOR data from plasma periods with no auxiliary heating applied in the JET pulse interval 71650-73999. Also shown is a fit to the data of the total spectrum obtained from an MCNPX run with the profile from JET pulse 73311 emitting as a thermonuclear 2.7 keV deuterium plasma. (Colour online)

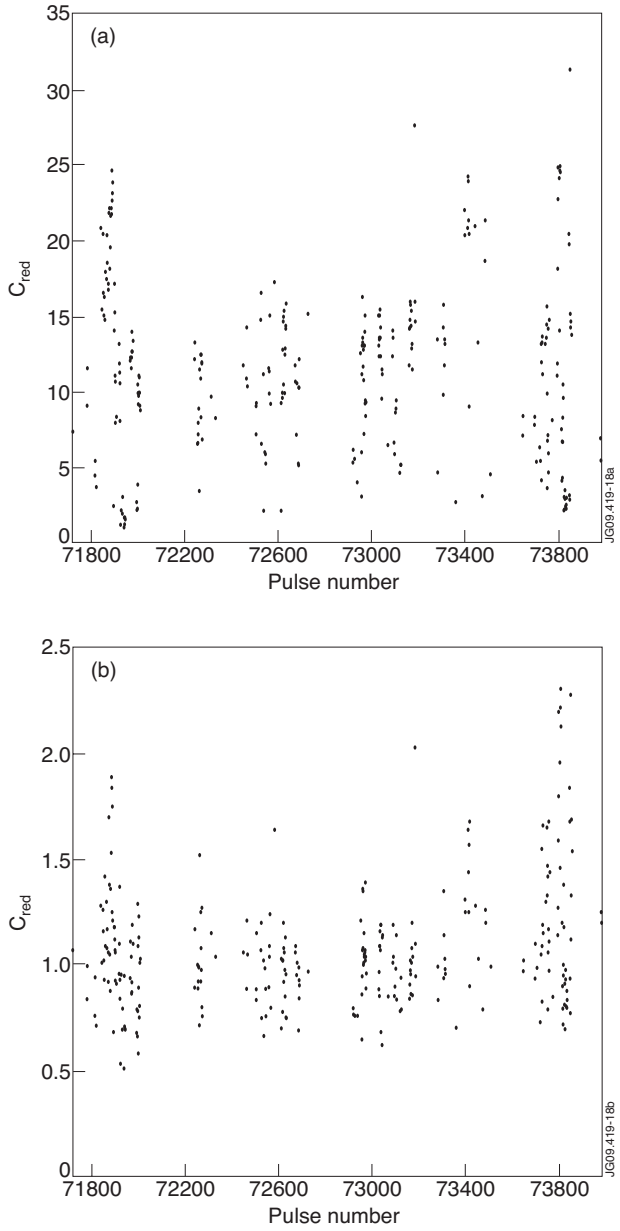

Figure 18: C*red from fits to NB heated JET pulses with* P_{NB}*>10 MW from the pulse interval 71650-73999 (a) without including a component to account for scattered neutrons in the fit and (b) with a scatter component. Note the different y-axis scales of the two panels.*

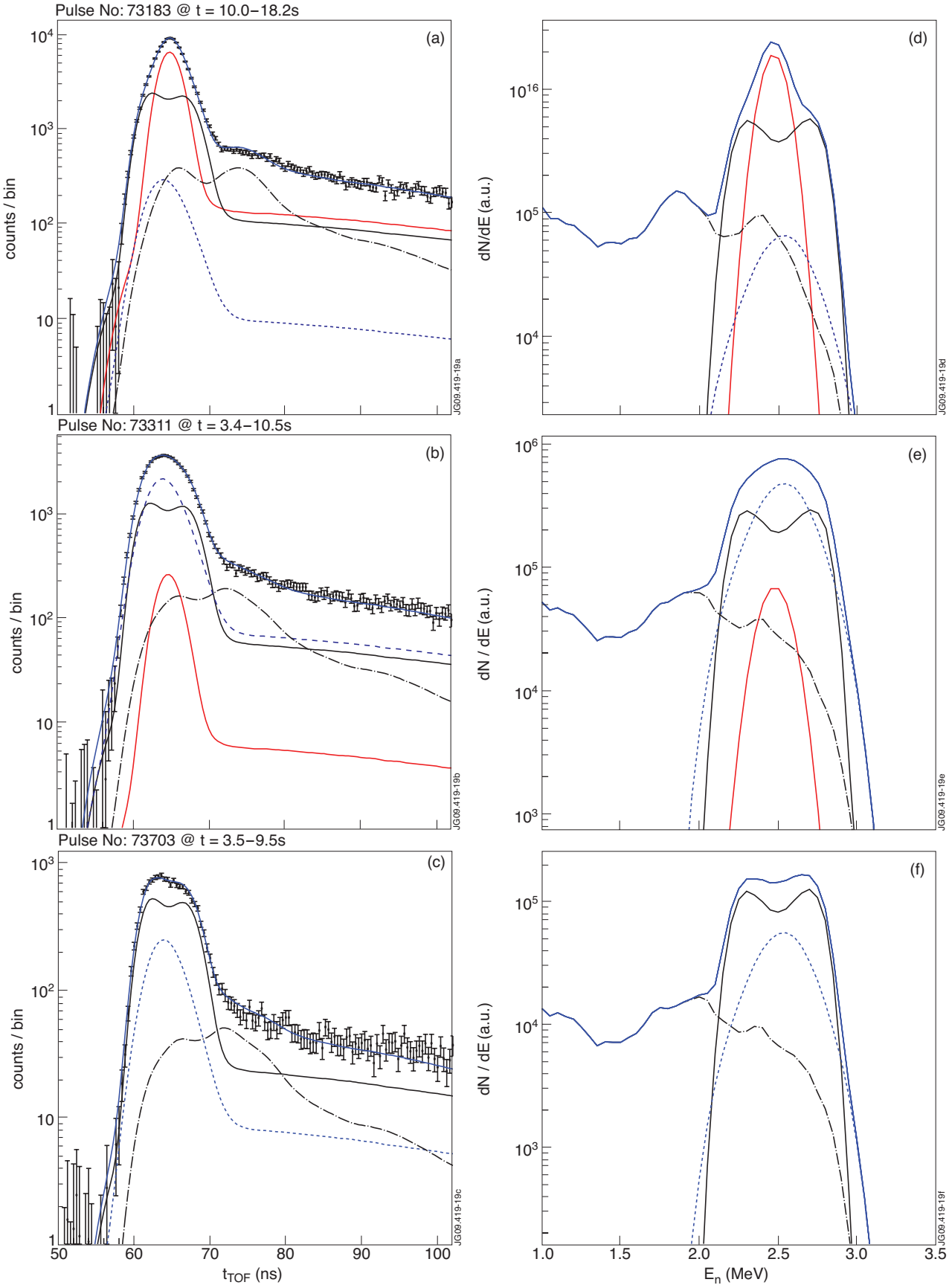

Figure 19: Examples of TOFOR data with the total fit (solid blue), thermal (solid red), beam-thermal (solid black), beam-beam (short dashed blue) and scatter (broken black) components indicated for JET Pulse No's: (a) 73183, (b) 73311 and (c) 73703. (d,e,f) show the fitted components on a neutron energy scale for Pulse No's: 73183, 73311 and 73703, respectively.

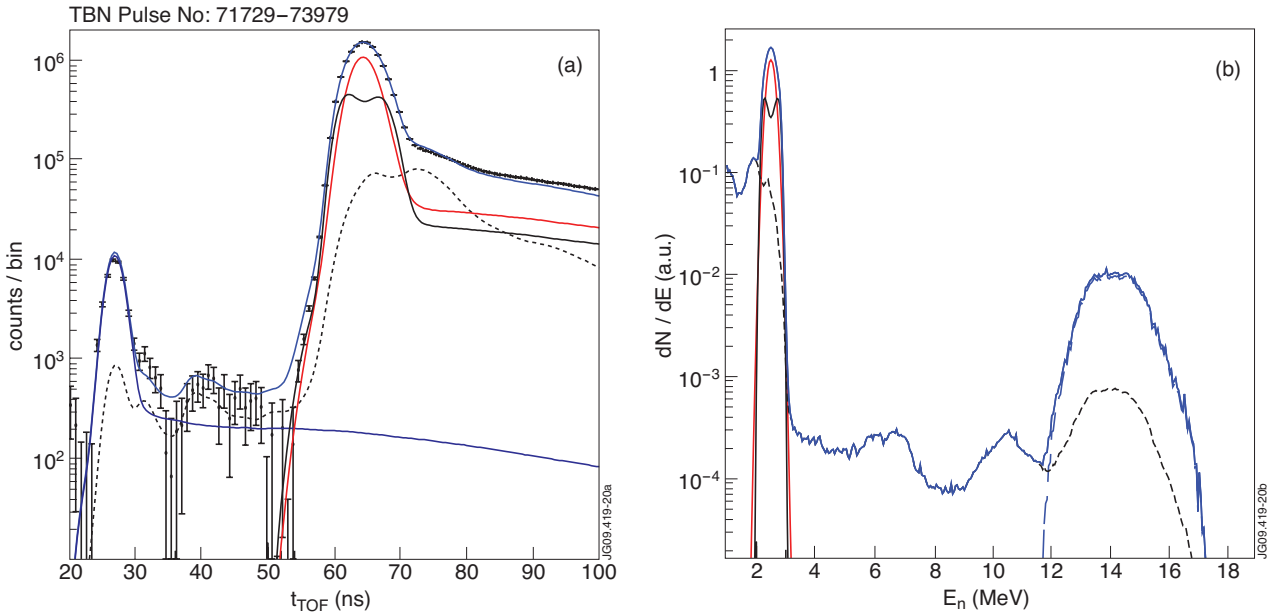

Figure 20: (a) Summed TOFOR data with fitted components and (b) the fitted components on a neutron energy scale from NB heated JET pulses with PNB>10 MW *in the interval 71650-73999. The data is fitted over a* t_{TOF} *interval including also the 14MeV neutron peak from d+t reactions, at 27ns in (a). Fitted components are thermal (solid red), beam-thermal (solid black), triton burn-up (long dashed blue) and scatter (dash-dot black). Also shown is the total fit to the data (solid blue).*

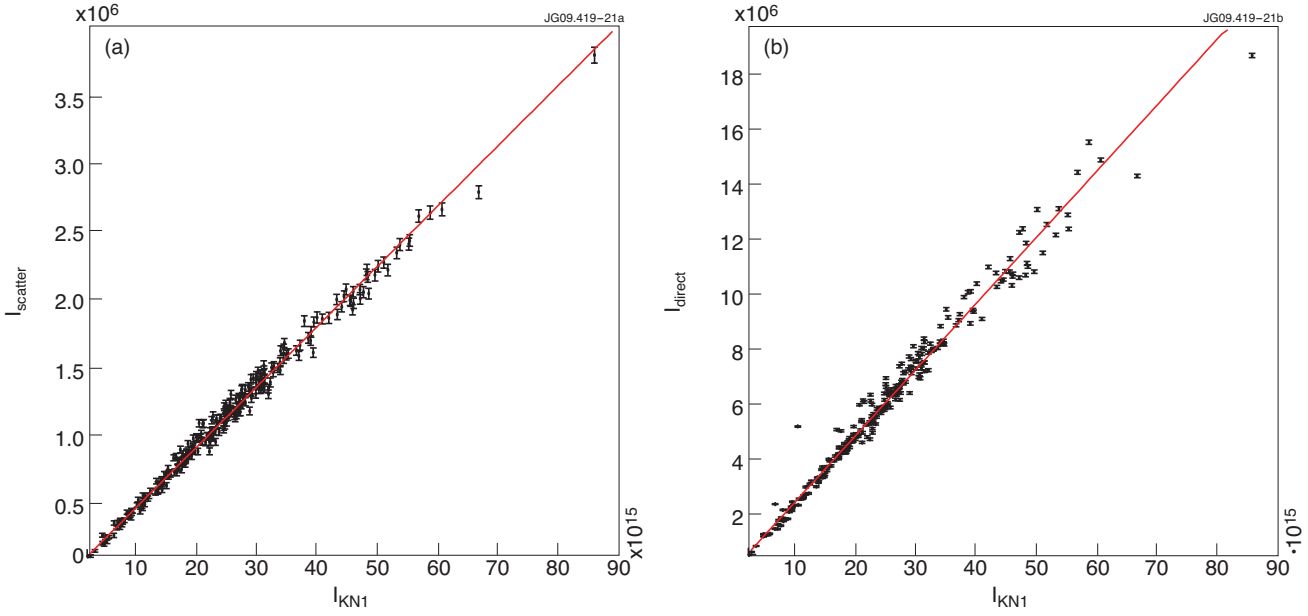

Figure 21: (a) Scattered and (b) direct neutrons incident on the primary TOFOR detector as determined from the fits to JET NB data in the interval 71650-74000, plotted as functions of the total number of neutrons emitted as obtained from the JET fission chambers (KN1). Also shown are fits to the data (solid red lines).

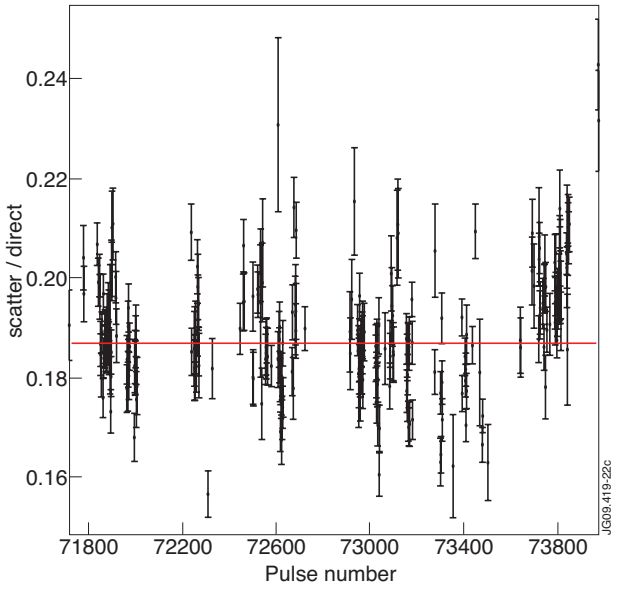

Figure 22. Scatter/direct ratio from fits to measured data as a function of pulse number for JET NB data (P_{NB}>10MW) from the pulse interval 71650-74000. Also shown is a 0-degree polynomial fit to the data (solid red line).

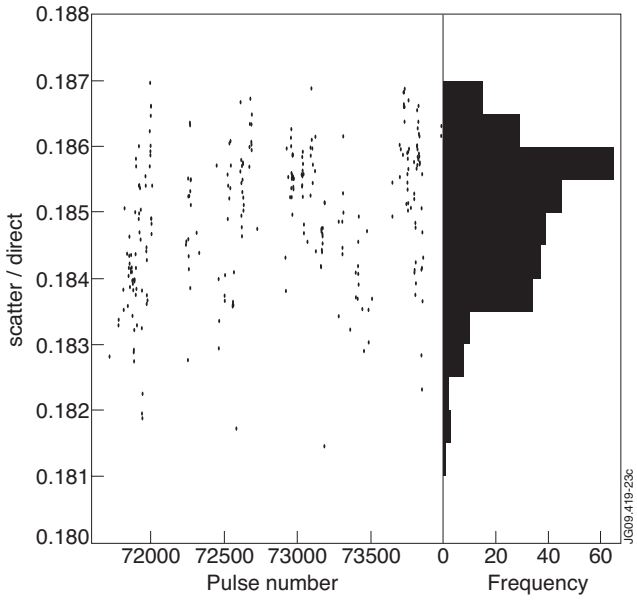

Figure 23: Expected variation in scatter/direct ratio due to variations in the direct spectrum shape, plotted as a function of pulse number (left) and as a frequency in scatter/direct space with bins of width 0.05 (right).

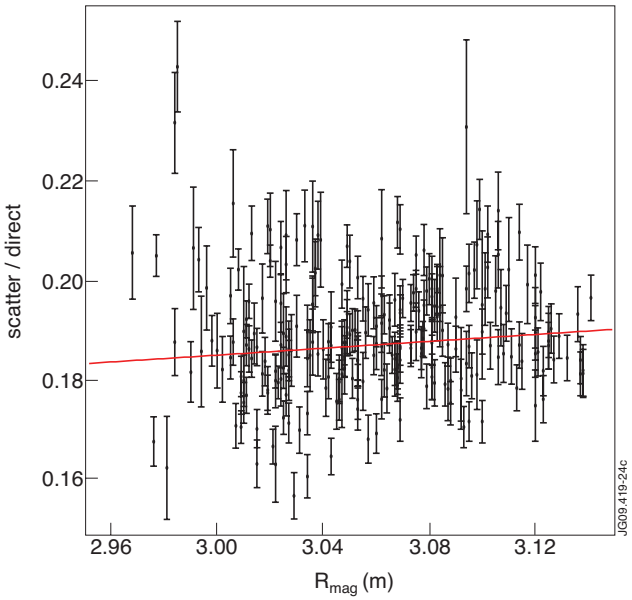

Figure 24: Scatter/direct ratio from fits to measured data as a function of average radial position of the magnetic axis (Rmag) for JET NB data (P_{NB}>10MW) from the pulse interval 71650-74000. Also shown is a fit to the data (solid red line).

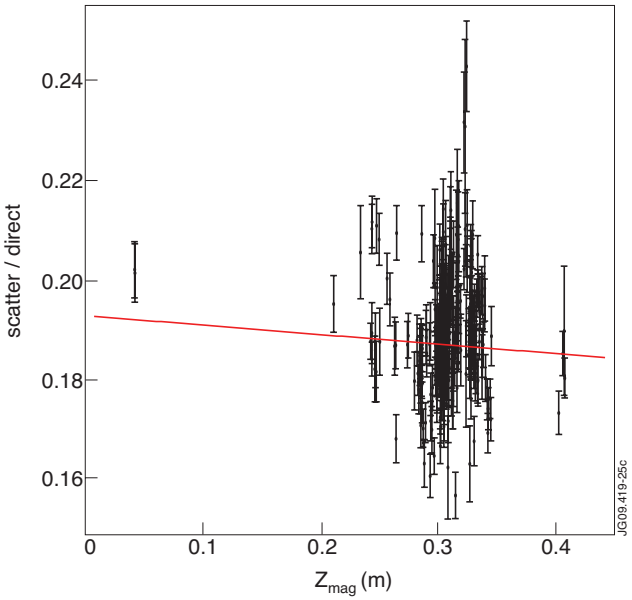

Figure 25: Scatter/direct ratio from fits to measured data as a function of average vertical position of the magnetic axis (Z_{mag}) for JET NB data (P_{NB}>10MW) from the pulse interval 71650-74000. Also shown is a fit to the data (solid red line).

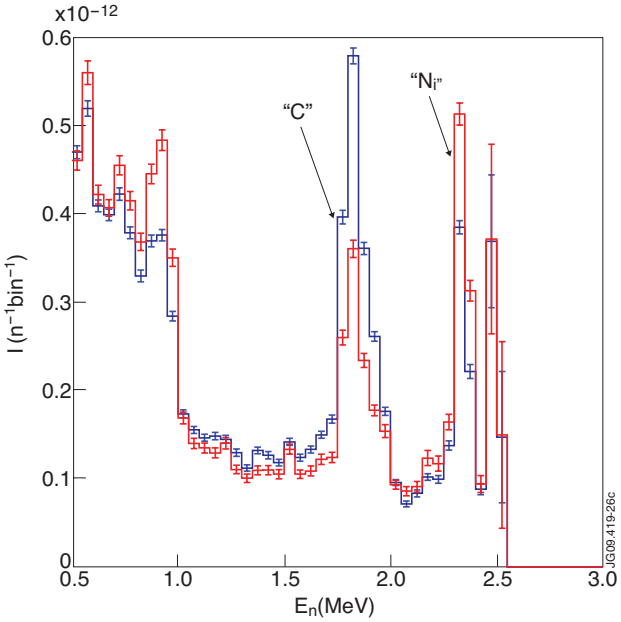

Figure 26: MCNPX scattered neutron spectra per cm^2 on the primary TOFOR detector (source neutron energy E=2.5±0.025MeV) with a material composition reflecting the current JET divertor structure (dashed blue) and the planned structure after the installation of the ILW (solid red), respectively.

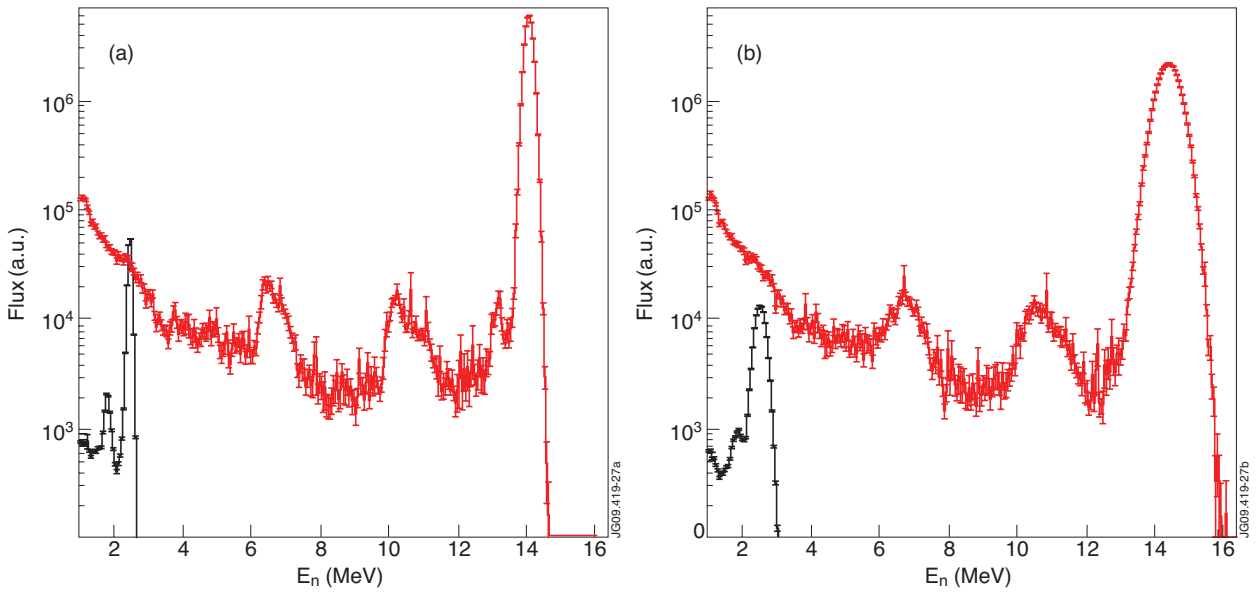

Figure 27: DD (black) and DT (red) neutron fluxes on TOFOR for (a) a 2.5keV and (b) a 20keV 50/50D/T plasma at JET, simulated using MCNPX. The relative neutron rates YDT/YDD are 210 in the 2.5keV case and 330 in the 20 keV case, as determined from the temperature dependent Maxwellian reactivites of the DD and DT reactions.